www.sciencemag.org/cgi/content/full/336/6085/1175/DC1

Supplementary Materials for

Generic Indicators for Loss of Resilience Before a Tipping Point Leading to Population Collapse

Lei Dai, Daan Vorselen, Kirill S. Korolev, Jeff Gore*

*To whom correspondence should be addressed. E-mail: gore@mit.edu

Published 1 June 2012, *Science* **336**, 1175 (2012)
DOI: 10.1126/science.1219805

This PDF file includes:

Materials and Methods

Experimental protocols

We used a yeast strain derived from haploid cells BY4741 (mating type **a**, EUROSCARF). All experiments were performed in 200 μl batch culture on BD Falcon 96-well Microtest plates at 30 ℃ using synthetic media (Yeast Nitrogen Bases + Nitrogen, Complete Supplement Mixture) supplemented with sucrose. Cultures were maintained in a well-mixed condition by growing in a shaker at 825 r.p.m. To avoid evaporation and contamination across wells, the plates were covered with Parafilm Laboratory Film. The 20% sucrose stock solution was filter-sterilized and stored with 1mM Tris buffer, pH 8.0, to prevent acid-catalyzed autohydrolysis. In all experiments we manually added a trace amount of glucose 0.001%, so that the monosaccharide concentration in sucrose stock (<0.0001%) can be ignored.

Serial dilutions were performed daily (23 hours of growth) with variable dilution factors. The eight dilution factors for the experimental data presented in Fig. 1 and Fig. 3 are 250, 500, 750, 1000, 1133, 1266, 1400 and 1600. Population densities were recorded each day before the serial dilution by measuring optical density at 620 nm using a Thermo Scientific Multiskan FC microplate photometer and periodically confirmed by plating (Figure S8).

Calculation of indicators

Statistical indicators were calculated at each observation time over an ensemble of replicate populations. The standard errors and confidence intervals of the indicators were given by bootstrap. The formulas of indicators and bootstrap procedures are presented in the next two sections.

In all the analysis we ensured environmental homogeneity by excluding populations with systematic differences in density, which are presumably caused by errors in daily dilution. For the eight dilution factors, the total number of replicate populations used for calculating indicators shown in Fig.3 is 70, 55, 56, 48, 46, 48, 49 and 48, respectively. Indicators calculated over the entire ensemble without imposing any selection display similar trends with larger increases (Figure S9).

Formula

1) Sample standard deviation: $s = \sqrt{\frac{1}{n-1}\sum_{i=1}^{n}(x_i - < x >)^2}$

   $< x >$: the sample mean.

2) Coefficient of variation: the sample standard deviation divided by the sample mean.

3) Sample skewness: $g_1 = \frac{m_3}{m_2^{3/2}}$

   m_3: the sample third central moment; m_2: the sample variance.

4) Autocorrelation time τ

The autocorrelation time τ was calculated as $\rho = e^{-1/\tau}$, where lag-1 autocorrelation ρ was estimated by the sample Pearson's correlation coefficient between the population densities at subsequent days over all replicate populations.

The sample Pearson's correlation coefficient:

$$\rho = \frac{1}{n-1}\frac{\sum_{i=1}^{n}(x_{i,t} - < x_t >)(x_{i,t+1} - < x_{t+1} >)}{s_{x_t} s_{x_{t+1}}}$$

$x_{i,t}$: sample *i* at day *t*; $< x_t >$: the sample mean at day *t*; s_{x_t}: the sample standard deviation at day *t*.

Negative lag-1 autocorrelation would be meaningless for calculation of autocorrelation time, so we made a cutoff at $\rho = 0$

$$\tau = \begin{cases} -\frac{1}{\ln(\rho)} & 0 < \rho < 1 \\ 0 & \rho \le 0 \end{cases}$$

An alternative estimator of autocorrelation time based on the definition of integrated autocorrelation time*(31)*, which does not require a cutoff for lag-1 autocorrelation at zero, leads to similar results (data not shown). We also used regression to estimate the lag-1 autocorrelation. Regression normalizes the covariance by $s_{x_t}{}^2$ (the sample

variance at day *t*) instead of $s_{x_t} s_{x_{t+1}}$ (the product of standard deviation at day *t* and day *t+1*)*(32)*. For our analysis both estimators yielded similar results (data not shown).

Bootstrap

We used bootstrap to calculate standard errors of indicators. Indicators shown in Fig. 3 are calculated based on an ensemble of replicate populations over a span of 5 days. In bootstrap, we resampled the replicates. For each resampled distribution, there are two alternative methods: (a) calculate the indicators for each day, and then average over 5 days; (b) combine the data over 5 days into a single distribution, and then calculate the indicators. Both methods yielded almost identical results (data not shown). The error bars shown in Fig. 3 are calculated using method (a) and denote standard errors of indicators with resampling 1,000 times.

Supplementary Text

Details of stochastic simulation

Our simulation is based on a stochastic difference equation:

$$n_{t+1} = n_t g(n_t + \varepsilon_1 n_t, \theta) \quad (1)$$

Population density at day *t*: n_t

Growth function: $g(n_t, \theta) = \frac{n_{t+1}}{n_t}$

Control variable: θ=Dilution factor

The growth function $g(n_t, \theta)$ is generated by the deterministic model of two-phase yeast growth (Figure S4) by setting the total growth time during each day as 23 hours. In the simulation, we used the same parameter values as the fitting parameters listed in Table S1.

We introduced the noise in daily dilution $\varepsilon_1 n_t$ as proportional to the population density. $\varepsilon_1 \sim N(0, \sigma_1^2)$ is a Gaussian random variable with standard deviation $\sigma_1 = 0.15$.

In different simulation runs, we observed clear signals of critical slowing down similar to that seen in experiments. The magnitude of increase in these indicators does not match perfectly with the experimental data, however, this is expected because: 1) our two-phase yeast growth model is an obvious simplification; 2) we only have crude estimates of the location of bifurcation and the magnitude of noise. The following derivations will provide a relationship between the indicators and the parameters in simulation.

Derivations of critical slowing down and warning signals

We define $n_{eq}(\theta)$ as the non-zero stable fixed point of population density. $x_t = n_t - n_{eq}$ is the deviation from the stable fixed point at day *t*.

The deterministic difference equation (without noise):

$$n_{t+1} = n_t g(n_t, \theta) \quad (2)$$

After Taylor expansion of the growth rate $g(n_t, \theta)$ at n_{eq} to the first order (ignoring $O(x^2)$) and then minus n_{eq} on both sides, it yields

$$x_{t+1} = (1 + g'(n_{eq}, \theta) n_{eq}) x_t = \rho(\theta) x_t \quad (3)$$

where $g'(n_{eq}, \theta) \equiv \left. \frac{dg(n, \theta)}{dn} \right|_{n=n_{eq}}$.

As dilution factor θ increases and approaches the bifurcation, $g'(n_{eq}, \theta)$ goes to zero (Figure S3), thus $\rho(\theta)$ goes to one. Also, we can transform Equation (3) to

$$x_{t+1} - x_t = -\lambda(\theta) x_t \quad (4)$$

It can be readily seen that the return rate of the system, $\lambda = 1 - \rho$, goes to zero upon reaching the bifurcation. This is the defining feature of critical slowing down.

After adding the two noise terms and performing a similar Taylor expansion for Equation (1) (only keeping the first order terms of x_t, ε_1), we get

$$x_{t+1} = \rho(\theta)x_t + \rho(\theta)n_{eq}(\theta)\varepsilon_1 \qquad (5)$$

This can be viewed as a first-order autoregressive (AR(1)) process*(8, 33)* with a Gaussian white noise at day *t*: $\varepsilon_t = \rho n_{eq}\varepsilon_1$. From Equation (5) we can derive the indicators: (< >: the expectation operator. See Materials and Methods: Calculation of indicators)

Mean: $< x_t >= 0$, $< n_t >= n_{eq}$

The lag-1 autocorrelation:

$$\frac{< (n_{t+1} - < n_{t+1} >)(n_t - < n_t >) >}{< (n_t - < n_t >)^2 >} = \frac{< x_{t+1}x_t >}{< x_t^2 >} = \rho(\theta)$$

$$\rho(\theta) = e^{-\Delta t/\tau} = e^{-1/\tau}, \quad \Delta t = 1$$

where τ is the autocorrelation time. Referring to our previous derivations of critical slowing down, we can see that upon approaching the bifurcation the lag-1 autocorrelation goes to one.

The return time τ_r satisfies (using Equation (3))

$$e^{-1/\tau_r} = \frac{x_{t+1}}{x_t} = \rho(\theta) = e^{-1/\tau}$$

Thus we can see that return time equals the autocorrelation time. They both diverge upon the approach of bifurcation.

Variance: $< (n_t - < n_t >)^2 >=< x_t^2 >= \frac{\rho^2 n_{eq}^2 \sigma_1^2}{1-\rho^2}$

Note $\rho = \rho(\theta), n_{eq} = n_{eq}(\theta)$.

Upon the approach of bifurcation, $\rho(\theta)$ goes to one, the standard deviation and coefficient of variation also diverge.

Thus, as the control parameter θ (dilution factor) is tuned to push the system closer to bifurcation, the lag-1 autocorrelation $\rho(\theta)$ goes to one and the autocorrelation time diverges; the standard deviation and coefficient of variation also diverge, and their divergence is inversely proportional to $\sqrt{1-\rho^2}$. The derivations and simulation results support that the increased variation and autocorrelation time observed in our experimental system before the fold bifurcation is indeed due to critical slowing down, and not due to any possible difference between the strength of noise introduced during daily dilution at different conditions.

Effects of measurement errors on indicators

Here we will briefly investigate the effects of measurement errors on indicators within the framework of our system. This could be an important issue in evaluating early

warning signals from noisy data sets, and we feel it has not been addressed explicitly in previous literature.

In our experiment, the measurement error comes from the measurement of optical density. It can be introduced as a Gaussian random variable $\varepsilon_2 \sim N(0, \sigma_2^2)$ with standard deviation $\sigma_2 \approx 2 \times 10^3$ cells/μl in our experiment (estimated by multiple measurements of optical density in the microplate photometer).

The indicators will then be calculated based on the measured values of population density on day *t*

$$\hat{n}_t = n_t + \varepsilon_2$$

The deviation from equilibrium is changed to $\hat{x}_t = x_t + \varepsilon_2$

Thus, there is an increase in variance

$$< (\hat{n}_t - < \hat{n}_t >)^2 >=< \hat{x}_t^2 >= \frac{\rho^2 n_{eq}^2 \sigma_1^2}{1-\rho^2} + \sigma_2^2$$

The covariance between different days is not changed

$$< \hat{x}_{t+1} \hat{x}_t >=< x_{t+1} x_t >$$

However, there is a decrease in lag-1 autocorrelation $\rho(\theta)$ because it is normalized by a larger variance now.

Given the relatively small measurement errors in our experimental system, the effects can be safely ignored. However, they could have notable effects on indicators based on field data with larger measurement errors.

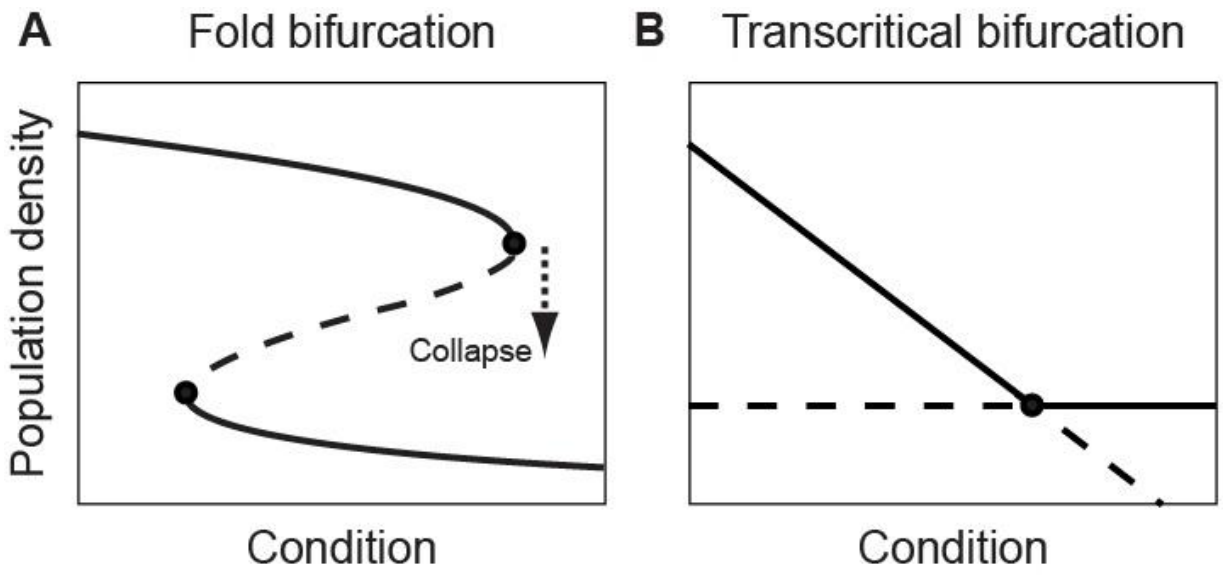

Figure S1. Catastrophic fold bifurcation vs. non-catastrophic transcritical bifurcation. The solid curves represent stable fixed points and the dashed curves represent unstable fixed points of a system. **(A)** If the curve of fixed points is folded backwards, the system can have two alternative stable states at a given condition. A fold bifurcation (solid circle) occurs when a stable fixed point and an unstable fixed point "collide" and annihalate*(8, 17)*. For a population subject to the strong Allee effect, there is a fold bifurcation in the population dynamics as the condition deteriorates. Crossing the fold bifurcation would result in a catastrophic population collapse. Due to hysteresis, reversing back to the former stable state after the catastrophic collapse can be difficult. **(B)** At a transcritical bifurcation (solid circle), a stable fixed point and an unstable fixed point meet and exchange stability. A transcritical bifurcation in population dynamics is a non-catastrophic threshold. It does not lead to a collapse (a large and sudden drop in population density) but rather a gradual decrease of population density as the condition deteriorates. Also, reversal is easy as there is only one stable fixed point in the system. Improving the condition back to the point just before the transcritical bifurcation would lead to an immediate recovery to the former stable state.

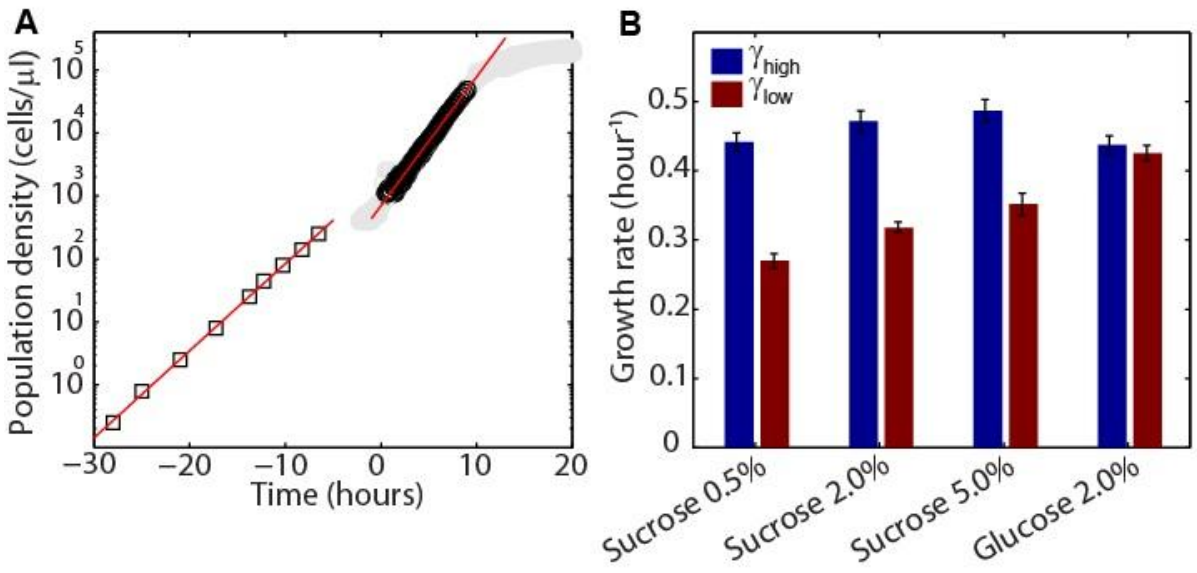

Figure S2. Measurement of per capita growth rate of yeast in sucrose at both low and intermediate cell densities. **(A)** Yeast populations were grown from a wide range of initial densities (0.25-2500 cells/µl) in 2% sucrose to estimate the growth rate at both low and intermediate cell densities*(27)*. Growth curves from different initial densities were superimposed (grey circles). We measured the growth rate at intermediate cell densities over the range of 10^3-5×10^4 cells/µl (black circles), giving $\gamma_{high} = 0.472 \pm .015$ hr^{-1} (standard error, n=8 independent measurements from different initial densities) in 2% sucrose. At higher densities the culture saturated upon reaching the carrying capacity. A yeast culture with population density smaller than ~10^3 cells/µl cannot be measured directly by absorbance in our microplate photometer. To measure the growth rate at low densities, we measured the time needed for the culture to reach a measurable density. The resulting locations of initial densities (black squares) allowed us to fit the growth rate at low cell densities $\gamma_{low} = 0.318 \pm .008$ hr^{-1} (95% confidence interval of the fitting parameter) in 2% sucrose, which is considerably lower than γ_{high}. The gap between the two growth phases in the graph is due to a lag phase when yeast cells adapt to the new media before starting growth. **(B)** In various sucrose concentrations, per capita growth rates of yeast at low densities (<10^3 cells//µl) γ_{low} is significantly lower than at intermediate densities (10^3-5×10^4 cells/µl) γ_{high}. At a higher sucrose concentration, γ_{low} increases and the difference between γ_{high} and γ_{low} decreases. As a control, in 2% glucose the growth rate of yeast is similar at low and intermediate densities.

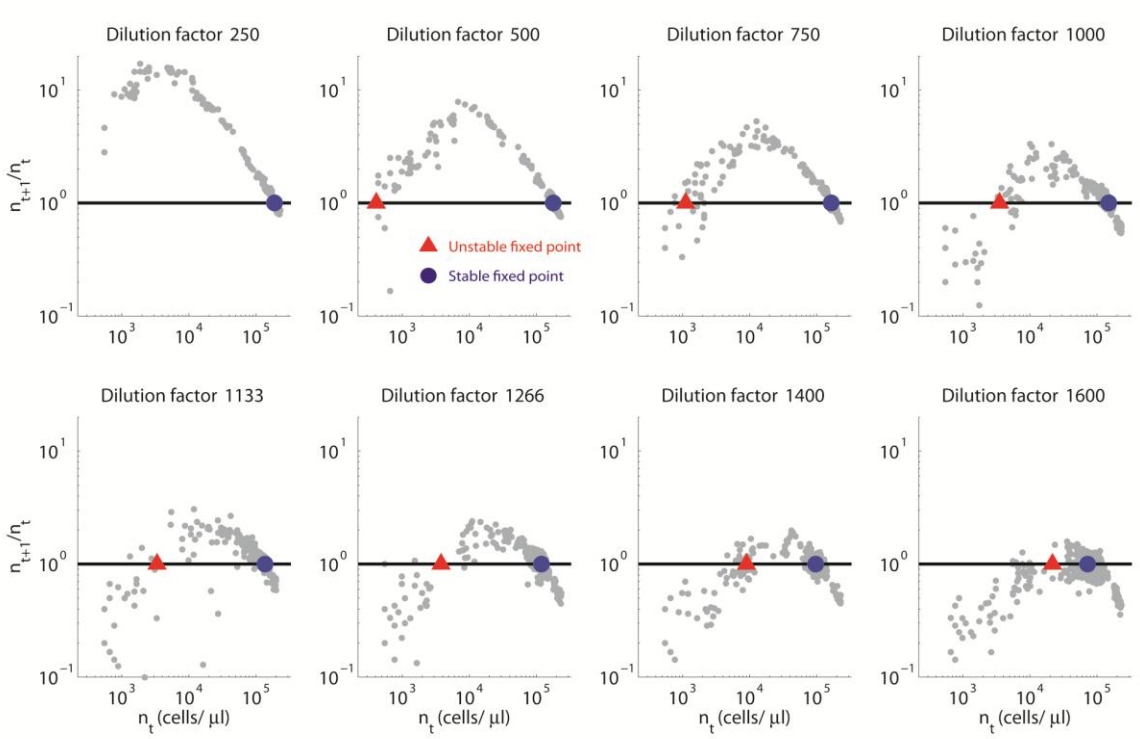

Figure S3. Identification of the stable and unstable fixed points at different conditions. The stable and unstable fixed points can be identified as fixed points at which the ratio of population densities between subsequent days $n_{t+1}/n_t = 1$ (solid line), n_t : population density at day t (t =1 to 6). The cooperative growth of yeast in sucrose leads to two stable fixed points, one close to saturation (blue circle) and the other one at extinction. There is an unstable fixed point (red triangle) in between. The populations are most fit at intermediate densities, thus displaying the Allee effect. The unstable fixed points are estimated by fitting the data points in the region where n_{t+1}/n_t is in the range of [0.5 2] and population density is between the detection limit (population density~5×10^2 cells/µl, below which the measurement becomes inaccurate) and the value that gives the maximum growth. Error bars of unstable fixed points shown in Fig. 1E correspond to 68% confidence interval of fitting parameters determined by bootstrap. The stable fixed points are estimated by the mean of replicate populations at equilibrium over five days and the error bars shown in Fig. 1E correspond to the standard deviation of day-to-day fluctuations.

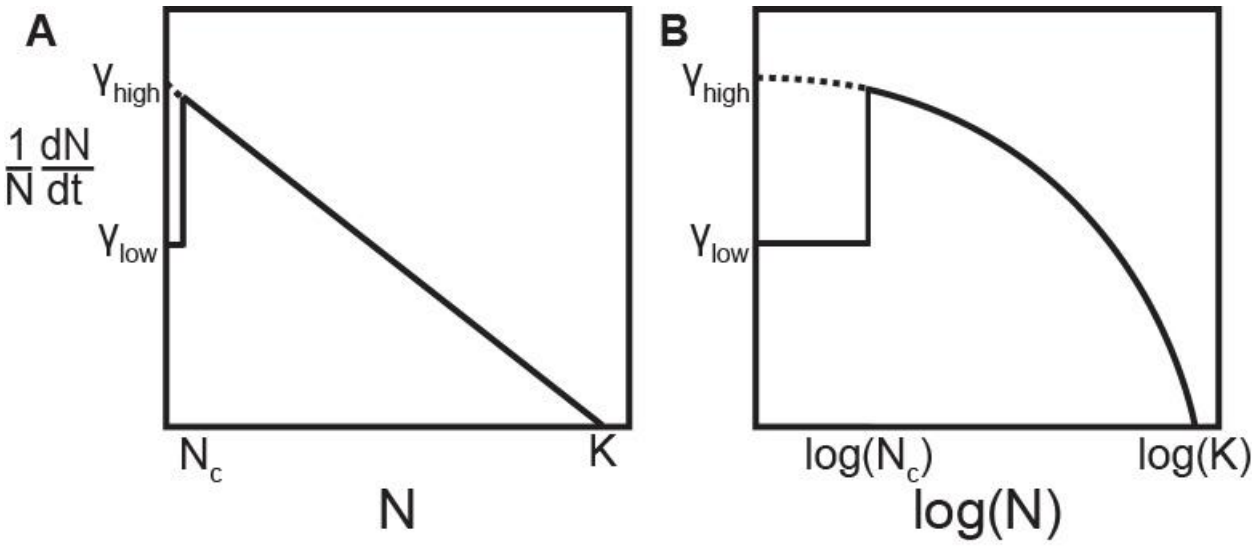

Figure S4. A simple deterministic model of two-phase yeast growth. Motivated by past measurements*(27)* and experimental data shown in Figure S2, we constructed a simple deterministic model to simulate yeast growth in sucrose. This model is based on two phases: a slow exponential growth phase at low cell densities, followed by a logistic growth phase with a higher per capita growth rate at intermediate cell densities. A schematic view of the per capita growth rate $\frac{1}{N}\frac{dN}{dt}$ as a function of the population density N is shown in **(A)** linear scale; **(B)** logarithmic scale. This model has five parameters: T_{lag} is the lag time before yeast cells start to grow after being transferred into new media. In the slow exponential phase, the population grows with a constant per capita growth rate γ_{low}. After the population reaches a threshold density N_c, the subsequent logistic growth is determined by γ_{high} ($\gamma_{high}>\gamma_{low}$) and the carrying capacity K.

$$\frac{1}{N}\frac{dN}{dt}=\begin{cases}\gamma_{low} & 0<N<N_c\\ \gamma_{high}(1-\frac{N}{K}) & N_c\le N<K\end{cases}$$

γ_{low}, γ_{high}, and K can be directly estimated by experiments. T_{lag} can be estimated indirectly. Details of estimation and comparisons between the fitting parameters used in Fig.1E and the experimental measured values are listed in Table S1.

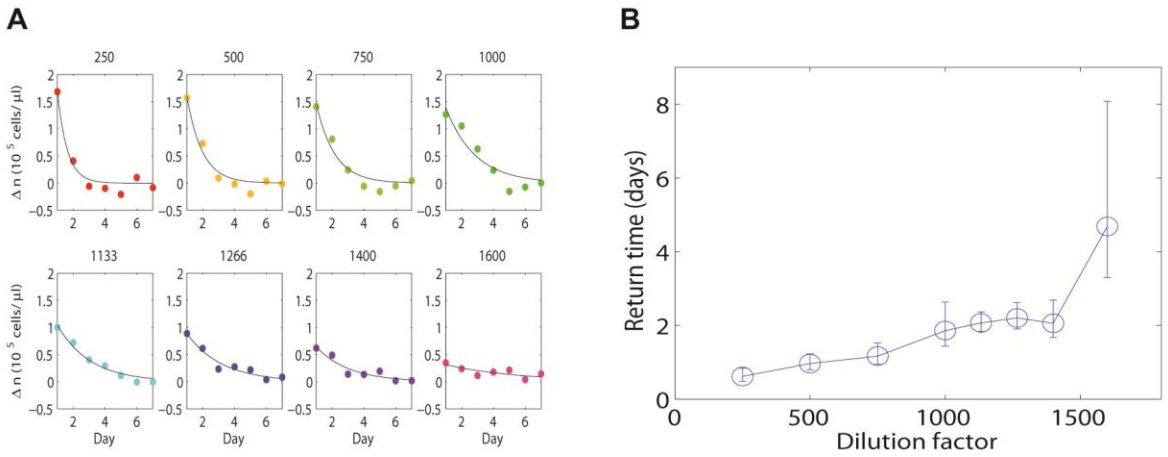

Figure S5. Estimated return time increases with dilution factor, consistent with the observation of critical slowing down. **(A)** We fit an exponential form $\Delta n(t) = c_1 \exp(-c_2 t)$ to the relaxation curves of populations starting at a certain initial density. $\Delta n = -(n_t - n_{eq})$ denotes the deviation from the stable fixed point n_{eq} at day *t*. Each data point is the average of eight replicate populations. Subplots are titled with the corresponding dilution factors. **(B)** Estimated return time $\tau = \frac{1}{c_2}$. The error bars represent 68% confidence interval of the fitting parameter. There is a clear increase in return time, consistent with the observation of critical slowing down. In principle, an exponential relaxation is expected when the deviation from equilibrium is assumed to be very small*(11, 18)*. The estimated return time by fitting the relaxation curves based on our experimental data could be inaccurate if the deviations are large enough to violate this assumption. Still, the increase in return time is significant and clear enough as an evidence of critical slowing down.

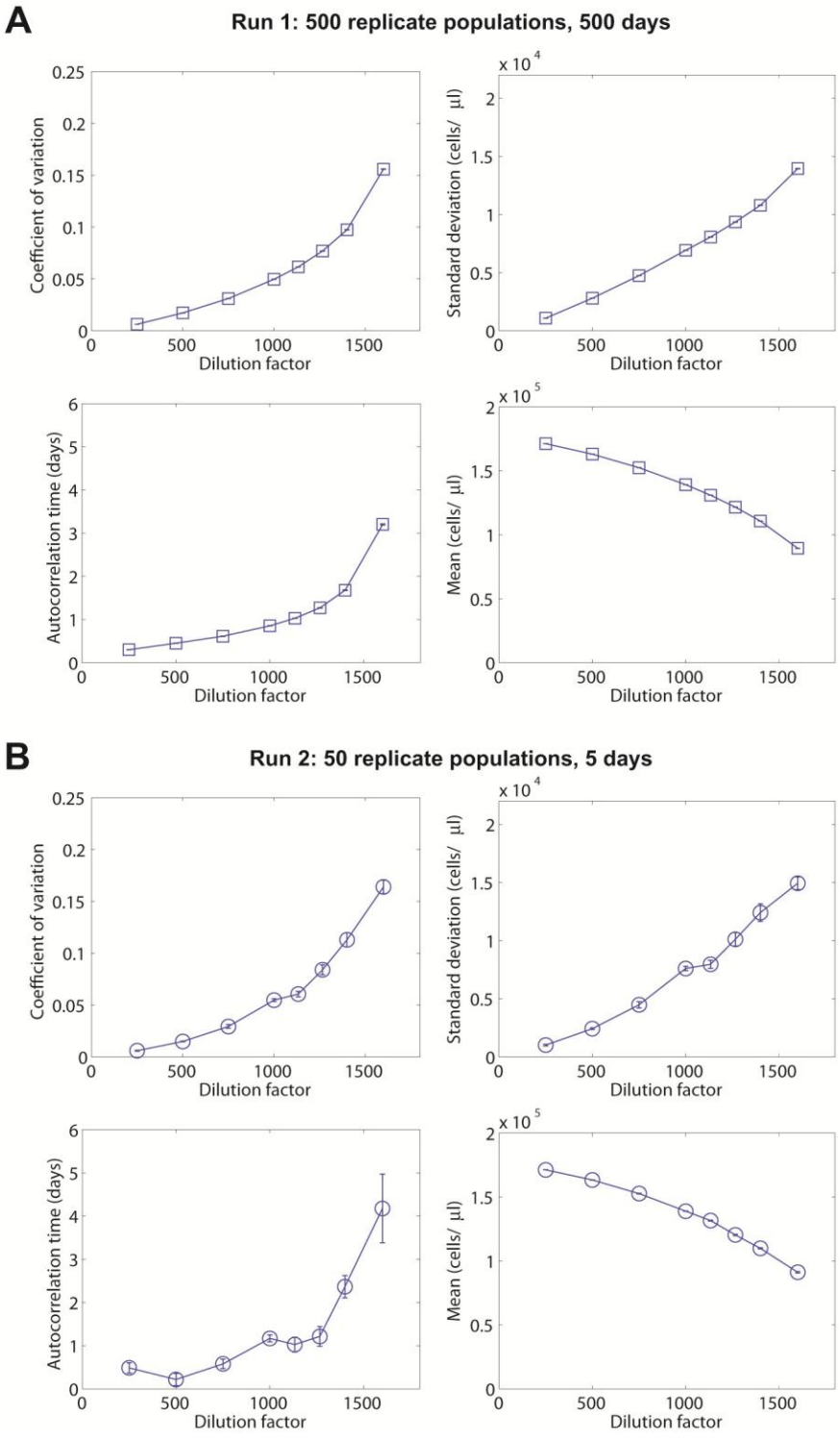

Figure S6. Indicators of critical slowing down appear in stochastic simulations. **(A)** Indicators in one simulation run with an ensemble of 500 replicate populations over a time span of 500 days. **(B)** Indicators in one simulation run with an ensemble of 50 replicate populations over a time span of 5 days (close to the sample size in our experimental setup). The mean population density of the ensemble is also shown. There is an initial period of 10 days to stabilize the populations. Error bars are standard errors of

day-to-day fluctuations. Histograms of population density in the two runs are shown in Figure S7. Details of stochastic simulation are given in the Supplementary Text.

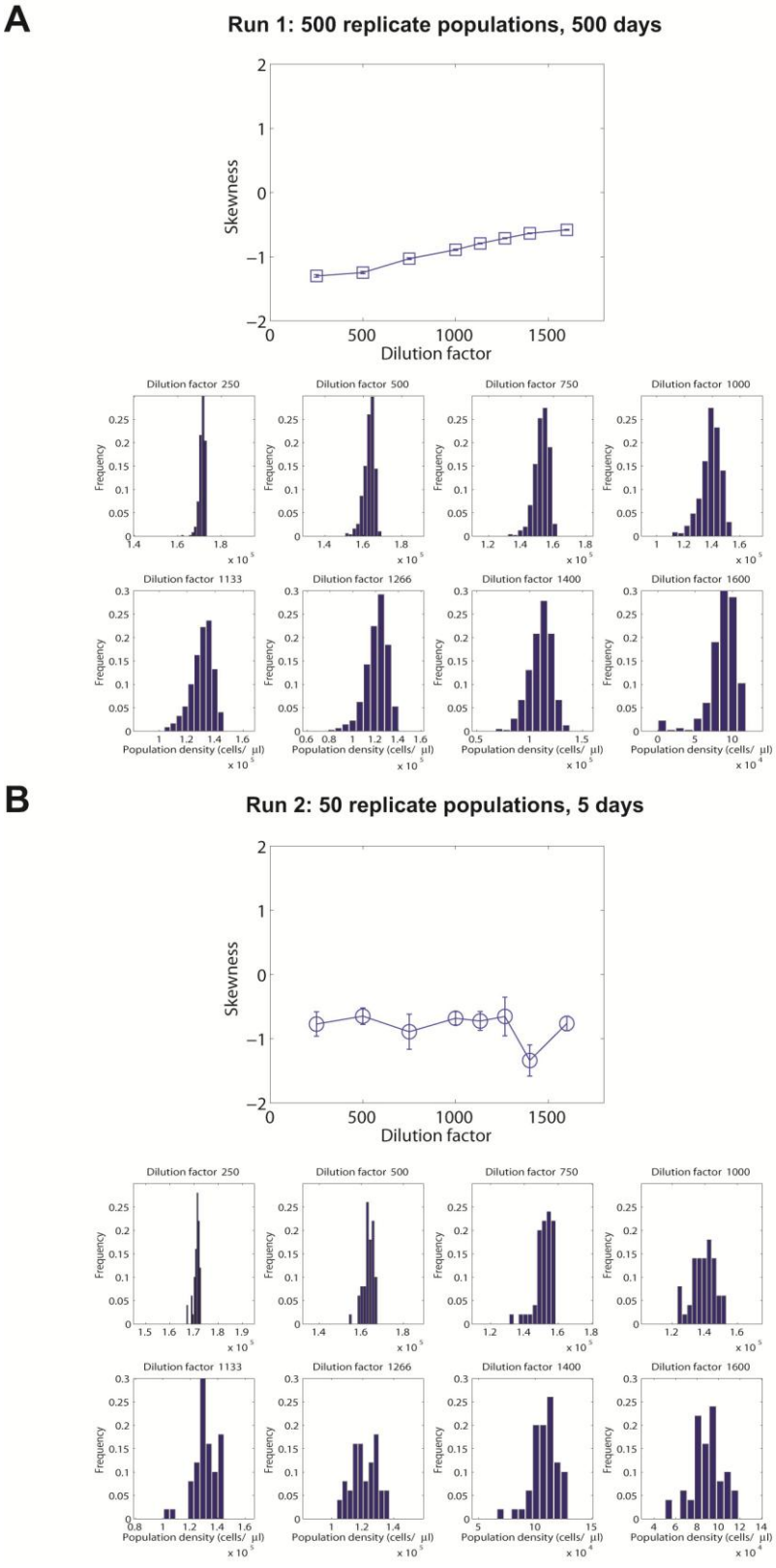

Figure S7. The magnitude of skewness decreases when approaching the bifurcation and shows large variation for small sample size. **(A)** One simulation run with an ensemble of

500 replicate populations over a time span of 500 days. Histogram of population density on the last day is shown. **(B)** One simulation run with an ensemble of 50 replicate populations over a time span of 5 days (close to the sample size in our experimental setup). Histogram of population density on the last day is shown. There is an initial period of 10 days to stabilize the populations. Error bars are standard errors of day-to-day fluctuations. The simulation adopted the same procedure as described in Figure S6. For the 500-day run, some populations at dilution factor 1600 went extinct stochastically and they were not included in the calculation of indicators in both Figure S6 and Figure S7. As shown in **(A)**, in simulation with a large sample size, the magnitude of skewness decreases when approaching the bifurcation, in contrast to previous theoretical arguments*(19)*. In **(B)**, the large variation in results suggests that no change in skewness should be detectable with the relatively small sample size in our experiments. Moreover, it will also be dependent on how skewed the perturbations or measurement errors are. Thus, we conclude that skewness is a good warning signal in our system.

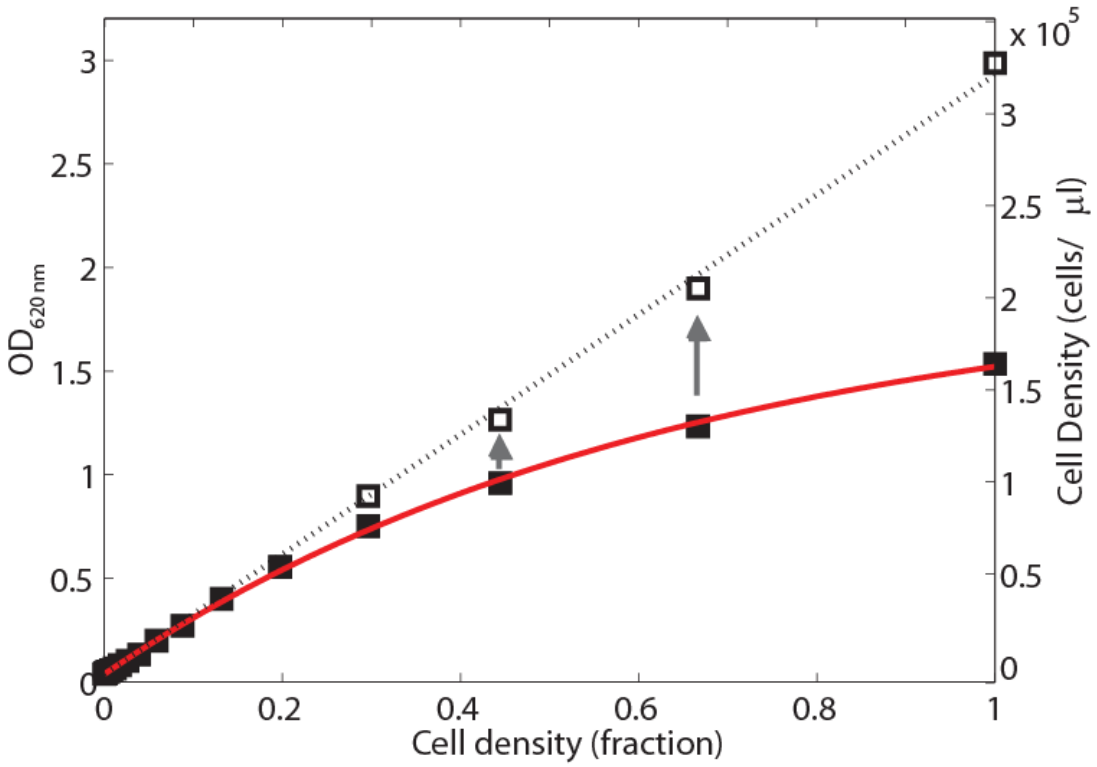

Figure S8. Calibration of optical density measurements and mapping to cell density. Population densities over three orders of magnitude were prepared by 17 serial dilution steps of 2/3 from an initial population at a highly saturated density. The fraction of the initial population density after each dilution step is shown on the x-axis. Optical density measurements were performed using a Thermo Multiskan FC microplate photometer at 620 nm. The measured optical density ($OD_{measured}$) of the instrument is linear with cell density up to ~ 0.3, while at higher densities $OD_{measured}$ saturates to a maximum value of recording. We use the following formula to transform the measured optical density $OD_{measured}$ (solid squares):

$$OD_{real} = -\ln[1 - \frac{OD_{measured} - OD_b}{OD_{\max} - OD_b}](OD_{\max} - OD_b)$$

where OD_b is the background recording of a sample without cells and $OD_{\max}$ is the maximum recording at saturating cell densities. In the calibration, we found $OD_b = 0.038$ and $OD_{\max} = 1.92$. After transformation, OD_{real} (open squares) reflects the real cell density given a recorded optical density $OD_{measured}$. OD_{real} is linear with cell density and plating experiments confirmed that $OD_{real} = 1$ corresponds to cell density $\approx 1.1 \times 10^5$ cells/µl. Measurements in a standard spectrophotometer with 1 cm light path at 600 nm (OD_{600}) showed that $OD_{600} = 5$ in the spectrometer is roughly equivalent to $OD_{real} = 1$ (data not shown).

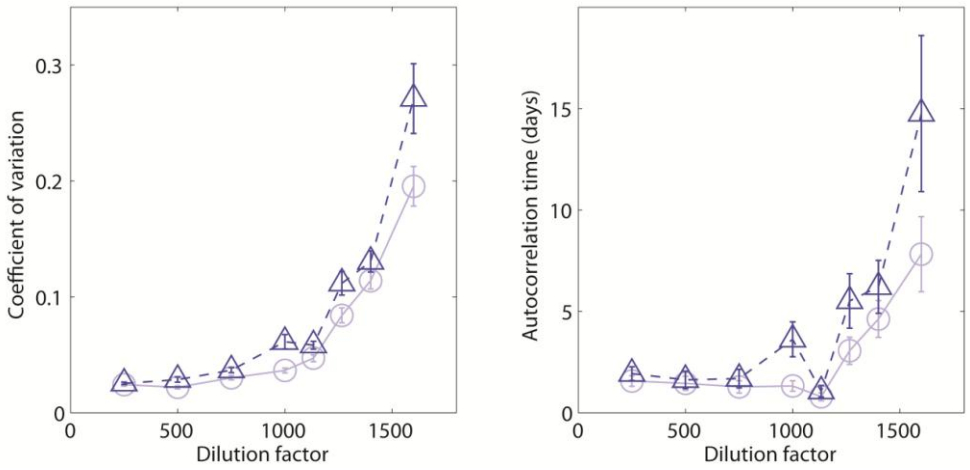

Figure S9. With an increasing dilution factor, statistical indicators calculated over either the entire ensemble or a subset of populations showed similar trends. Comparison between statistical indicators calculated using all the replicate populations (dark blue triangles) and using a subset of populations (light blue circles, data shown in Fig.3) for conditions of fixed dilution factors. The increase of indicators at high dilution factors based on all the replicate populations was even more significant. In the subset of populations, some wells on the edges of 96-well plates or displaying large jumps of population density ($>2\times10^4$ cells/μl) between subsequent days, presumably caused by pipetting errors, were excluded. For the eight dilution factors, the total number of replicate populations without imposing any selection is 80, 64, 64, 56, 56, 56, 56 and 48, respectively.

Table S1. Comparison between fitting parameters and experimentally measured values. The model parameters are explained in Figure S4. Fitting parameters are the values used for a typical fit of the bifurcation diagram shown in Figure 1e. γ_{high} and γ_{low} are determined experimentally as explained in Figure S2. K, the carrying capacity, is determined by taking the average density of ten saturated populations measured over an interval of five hours. T_{lag}, the time before yeast cells start growing in the new media, can be estimated indirectly from the following equation (right after the lag period, cells starting at intermediate densities approximately follow an exponential growth with growth rate γ_{high}):

$$\log(N_t) = \log(N_0) + (t - T_{lag})\gamma_{high} \qquad t \geq T_{lag}$$

where N_t is the measured population density at time t and N_0 the initial population density ($>10^3$ cells/μl). We cannot measure the threshold density N_c directly, as it is below the detection limit of our microplate photometer; an indirect estimate dependent on γ_{low}, γ_{high} and T_{lag} would be inaccurate.

We note that the two-phase yeast growth model is a simplified description of reality so it is not surprising that the parameter agreement is not perfect. However, the fit of the experimental bifurcation diagram (Fig.1E) and the observation of critical slowing down signals in stochastic simulations being consistent with experimental data (Figure S6) merit the model as a reasonable approximation of reality, which captures the cooperative feature of yeast growth dynamics in sucrose.

	Measured values	Fitting parameters
γ_{high}	$0.472 \pm .015$ hr^{-1}	0.439 hr^{-1}
γ_{low}	$0.318 \pm .008$ hr^{-1}	0.309 hr^{-1}
K	$1.95 \pm .13 \times 10^5$ cells/μl	1.76×10^5 cells/μl
T_{lag}	2.58 hr	2.97 hr
N_c	-	2.76×10^2 cells/μl

References

1. J. A. Hutchings, J. D. Reynolds, Marine fish population collapses: Consequences for recovery and extinction risk. *Bioscience* **54**, 297 (2004). doi:10.1641/0006-3568(2004)054[0297:MFPCCF]2.0.CO;2

2. K. T. Frank, B. Petrie, J. A. Fisher, W. C. Leggett, Transient dynamics of an altered large marine ecosystem. *Nature* **477**, 86 (2011). doi:10.1038/nature10285 Medline

3. M. Scheffer, *Critical Transitions in Nature and Society* (Princeton Univ. Press, Princeton, NJ, 2009).

4. M. Scheffer, S. Carpenter, J. A. Foley, C. Folke, B. Walker, Catastrophic shifts in ecosystems. *Nature* **413**, 591 (2001). doi:10.1038/35098000 Medline

5. R. M. May, Thresholds and breakpoints in ecosystems with a multiplicity of stable states. *Nature* **269**, 471 (1977). doi:10.1038/269471a0

6. T. M. Lenton *et al*., Tipping elements in the Earth's climate system. *Proc. Natl. Acad. Sci. U.S.A.* **105**, 1786 (2008). doi:10.1073/pnas.0705414105 Medline

7. C. S. Holling, Resilience and stability of ecological systems. *Annu. Rev. Ecol. Syst.* **4**, 1 (1973). doi:10.1146/annurev.es.04.110173.000245

8. M. Scheffer *et al*., Early-warning signals for critical transitions. *Nature* **461**, 53 (2009). doi:10.1038/nature08227 Medline

9. T. M. Lenton, Early warning of climate tipping points. *Nat. Clim. Change* **1**, 201 (2011). doi:10.1038/nclimate1143

10. S. R. Carpenter, W. A. Brock, Rising variance: A leading indicator of ecological transition. *Ecol. Lett.* **9**, 311 (2006). doi:10.1111/j.1461-0248.2005.00877.x Medline

11. E. H. van Nes, M. Scheffer, Slow recovery from perturbations as a generic indicator of a nearby catastrophic shift. *Am. Nat.* **169**, 738 (2007). doi:10.1086/516845 Medline

12. J. M. Drake, B. D. Griffen, Early warning signals of extinction in deteriorating environments. *Nature* **467**, 456 (2010). doi:10.1038/nature09389 Medline

13. S. R. Carpenter *et al*., Early warnings of regime shifts: A whole-ecosystem experiment. *Science* **332**, 1079 (2011). doi:10.1126/science.1203672 Medline

14. V. Dakos *et al*., Slowing down as an early warning signal for abrupt climate change. *Proc. Natl. Acad. Sci. U.S.A.* **105**, 14308 (2008). doi:10.1073/pnas.0802430105 Medline

15. A. Hastings, D. B. Wysham, Regime shifts in ecological systems can occur with no warning. *Ecol. Lett.* **13**, 464 (2010). doi:10.1111/j.1461-0248.2010.01439.x Medline

16. A. J. Veraart *et al*., Recovery rates reflect distance to a tipping point in a living system. *Nature* **481**, 357 (2012). Medline

17. S. H. Strogatz, *Nonlinear Dynamics and Chaos: With Applications to Physics, Biology, Chemistry, and Engineering* (Westview, Boulder, CO, 1994).

18. C. Wissel, A universal law of the characteristic return time near thresholds. *Oecologia* **65**, 101 (1984). doi:10.1007/BF00384470

19. V. Guttal, C. Jayaprakash, Changing skewness: An early warning signal of regime shifts in ecosystems. *Ecol. Lett.* **11**, 450 (2008). doi:10.1111/j.1461-0248.2008.01160.x Medline

20. J. P. Scholz, J. A. S. Kelso, G. Schöner, Nonequilibrium phase transitions in coordinated biological motion: Critical slowing down and switching time. *Phys. Lett. A* **123**, 390 (1987). doi:10.1016/0375-9601(87)90038-7

21. P. D. H. Hines, E. Cotilla-Sanchez, B. O'hara, C. Danforth, in *2011 IEEE Power and Energy Society General Meeting* (IEEE, Detroit, 2011), pp. 1–5.

22. W. C. Allee, A. E. Emerson, O. Park, T. Park, K. P. Schmidt, *Principles of Animal Ecology* (Saunders, Philadelphia, 1949).

23. F. Courchamp, T. Clutton-Brock, B. Grenfell, Inverse density dependence and the Allee effect. *Trends Ecol. Evol.* **14**, 405 (1999). doi:10.1016/S0169-5347(99)01683-3 Medline

24. P. A. Stephens, W. J. Sutherland, Consequences of the Allee effect for behaviour, ecology and conservation. *Trends Ecol. Evol.* **14**, 401 (1999). doi:10.1016/S0169-5347(99)01684-5 Medline

25. T. Coulson, G. M. Mace, E. Hudson, H. Possingham, The use and abuse of population viability analysis. *Trends Ecol. Evol.* **16**, 219 (2001). doi:10.1016/S0169-5347(01)02137-1 Medline

26. P. M. Groffman *et al*., Ecological thresholds: The key to successful environmental management or an important concept with no practical application? *Ecosystems* **9**, 1 (2006). doi:10.1007/s10021-003-0142-z

27. J. Gore, H. Youk, A. van Oudenaarden, Snowdrift game dynamics and facultative cheating in yeast. *Nature* **459**, 253 (2009). doi:10.1038/nature07921 Medline

28. See supplementary materials on *Science* Online.

29. C. Folke *et al*., Regime shifts, resilience, and biodiversity in ecosystem management. *Annu. Rev. Ecol. Evol. Syst.* **35**, 557 (2004). doi:10.1146/annurev.ecolsys.35.021103.105711

30. L. H. Gunderson, Ecological resilience in theory and application. *Annu. Rev. Ecol. Syst.* **31**, 425 (2000). doi:10.1146/annurev.ecolsys.31.1.425

31. C. B. Lang, *Data Survival Guide* (http://physik.uni-graz.at/~cbl/teaching/dsg/dsg.html).

32. D. Freedman, R. Pisani, R. Purves, *Statistics* (Norton, New York, 2007).

33. A. R. Ives, Measuring resilience in stochastic systems. *Ecol. Monogr.* **65**, 217 (1995). doi:10.2307/2937138